DOI: 10.1002/chem.200601759

# Unmasking Melon by a Complementary Approach Employing Electron Diffraction, Solid-State NMR Spectroscopy, and Theoretical Calculations—Structural Characterization of a Carbon Nitride Polymer

**Bettina V. Lotsch,[a] Markus Döblinger,[a] Jan Sehnert,[b] Lena Seyfarth,[b] Jürgen Senker,*[b] Oliver Oeckler,[a] and Wolfgang Schnick*[a]**

*Dedicated to Professor Wolfgang Beck on the occasion of his 75th birthday*

**Abstract:** Poly(aminoimino)heptazine, otherwise known as Liebig's melon, whose composition and structure has been subject to multitudinous speculations, was synthesized from melamine at 630 °C under the pressure of ammonia. Electron diffraction, solid-state NMR spectroscopy, and theoretical calculations revealed that the nanocrystalline material exhibits domains well-ordered in two dimensions, thereby allowing the structure solution in projection by electron diffraction. Melon ($[C_6N_7(NH_2)(NH)]_n$, plane group $p2gg$, $a=16.7$, $b=12.4$ Å, $\gamma=90°$, $Z=4$), is composed of layers made up from infinite 1D chains of NH-bridged melem ($C_6N_7(NH_2)_3$) monomers. The strands adopt a zigzag-type geometry and are tightly linked by hydrogen bonds to give a 2D planar array. The inter-layer distance was determined to be 3.2 Å from X-ray powder diffraction. The presence of heptazine building blocks, as well as NH and $NH_2$ groups was confirmed by $^{13}C$ and $^{15}N$ solid-state NMR spectroscopy using $^{15}N$-labeled melon. The degree of condensation of the heptazine core was further substantiated by a $^{15}N$ direct excitation measurement. Magnetization exchange observed between all $^{15}N$ nuclei using a fp-RFDR experiment, together with the CP-MAS data and elemental analysis, suggests that the sample is mainly homogeneous in terms of its basic composition and molecular building blocks. Semiempirical, force field, and DFT/plane wave calculations under periodic boundary conditions corroborate the structure model obtained by electron diffraction. The overall planarity of the layers is confirmed and a good agreement is obtained between the experimental and calculated NMR chemical shift parameters. The polymeric character and thermal stability of melon might render this polymer a pre-stage of g-$C_3N_4$ and portend its use as a promising inert material for a variety of applications in materials and surface science.

**Keywords:** ab initio calculations · carbon nitrides · electron diffraction · solid-state NMR spectroscopy · solid-state structures

## Introduction

The quest for binary carbon nitride $C_3N_4$, whose postulated material properties are believed to push the borders of ultra-hard materials, has provided a tight link between Liebig's historic work and modern materials chemistry.[1] While being re-invented in a new context in the 1980s, carbon nitride had been discussed as the ultimate de-ammonation product of a series of "ammonocarbonic acids" such as cyanamide or melamine as early as 1834.[2] All attempts to synthesize pure carbon nitride were invariably spoiled by the presence of hydrogen, yielding an amorphous, infusible material which was first obtained by Berzelius and given the name "melon" by Liebig.[2,3] As reviewed by Franklin,[3] the latter was obtained by heating to redness the yellow precipi-

[a] Dr. B. V. Lotsch, Dr. M. Döblinger, Dr. O. Oeckler, Prof. Dr. W. Schnick
Department Chemie und Biochemie
Ludwig-Maximilians-Universität
Butenandtstrasse 5–13 (D), 81377 München (Germany)
Fax: (+49) 89-2180-77440
E-mail: wolfgang.schnick@uni-muenchen.de

[b] J. Sehnert, L. Seyfarth, Prof. Dr. J. Senker
Anorganische Chemie I
Universität Bayreuth
Universitätsstrasse 30, 95447 Bayreuth (Germany)
Fax: (+49) 921-55-2788
E-mail: juergen.senker@uni-bayreuth.de

Supporting information for this article is available on the WWW under http://www.chemeurj.org/ or from the author.

  

tate formed by the action of chlorine on a solution of potassium or sodium thiocyanate, by heating ammonium or mercury thiocyanate, and as the final de-ammonation product on heating mixed "aquo-ammonocarbonic acids" such as ammeline or urea.[4,5] Owing to its unusual thermal stability, some doubt arose whether melon should be classified as an organic or an inorganic compound. Despite the lack of sharply defined composition, melon was assigned the empirical formula $H_3C_6N_9$, which led Redemann and Lucas to draw two alternative planar structure models based on the heptazine (cyameluric) core $C_6N_7$ (Scheme 1, **1a** + **1b**). Alternatively, a symmetric triangular form was proposed, whose empirical formula approaches asymptotically the limit $C_3N_4$ if condensations extend indefinitely (Scheme 1, **1c**).[4]

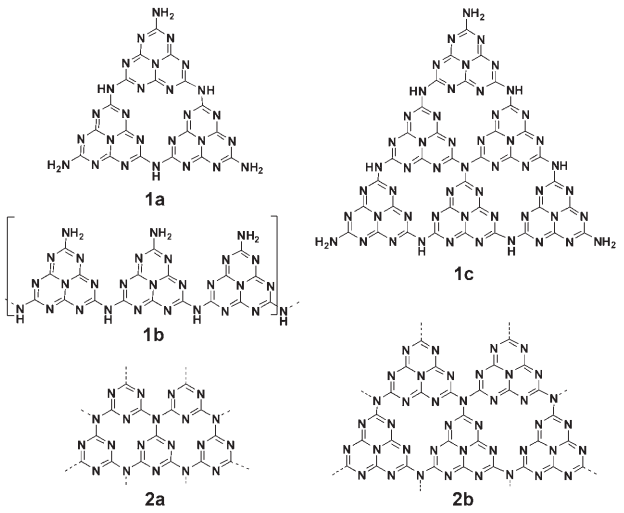


Scheme 1. Structure models proposed for melon (**1a**, **1b**) and cutouts of hypothetical structure models of graphitic carbon nitride based on triazine (**2a**) and heptazine building blocks (**2b**). The melon-derived structure "$C_{36}N_{52}H_{12}$" (**1c**) has an empirical formula intermediate between melon and g-$C_3N_4$.

Other structure models, including triazine-based variants, have been put forward for melon owing to the lack of detailed knowledge on the structure of its presumed monomer, melem.[6] Franklin found that the empirical composition of melon varied with the method of preparation, as he obtained samples with a hydrogen content between 1.1 and 2.0 wt%. Products with a hydrogen content of only 0.6 wt% were rationalized by assuming a mixture of several "compact" condensation products of triangular shape as for example model **1c** (Scheme 1).[3,4a] On this background, it was conjectured that "it is probably incorrect to assign any one structure to melon, for it is more than likely a mixture of molecules of different sizes and shapes. This gives rise to its amorphous character".[4a]

The gap between historic and modern carbon nitride chemistry is bridged by the hypothetical graphitic modification of $C_3N_4$ (g-$C_3N_4$), which has been calculated to be the most stable form of carbon nitride, and owing to its analogy with graphite was attributed the triazine core $C_3N_3$ as elementary building block (Scheme 1, **2a**).[1,7] Since then, a plethora of experimental and theoretical efforts have been made to elucidate the structure of g-$C_3N_4$, which failed due to the ill-defined nature of the obtained polymers.[7,8]

The search for graphitic carbon nitride typically emanates from derivatives or precursors of triazine, whose structural integrity is believed to be preserved upon thermal treatment of the starting materials. Thus, a considerable number of possible triazine-based structures—akin to graphite—has been devised and their topologies as well as their relative stabilities computed.[1d,8,10,11] For example, Kawaguchi et al. synthesized a material with the presumed formula $[(C_3N_3)_2(NH)_3]_n$ ($\equiv C_6N_9H_3$) by polycondensation of cyanuric chloride and melamine, whose electron diffraction pattern was indexed on a hexagonal cell with $a = 8.2$ Å and $d_{100} = 7.1$ Å.[7b] Demazeau et al. reported on the solvothermal synthesis of g-$C_3N_4$ by reacting melamine with hydrazine as a nitriding agent under supercritical conditions.[7a,g,l,o,11]

Only recently, an alternative structure model based on the heptazine nucleus emerged (**2b**, Scheme 1), reminiscent of the extensive work on melon, which still represents a highly controversial chapter in the history of C/N chemistry.[8a,12–15] Although the heptazine-based nitrogen compounds such as melem or cyameluric acid had been known for decades, the significantly less stable unsubstituted nucleus, tri-*s*-triazine, was synthesized and structurally characterized only in the 1980s.[16] Komatsu proposed polymers of melem to form upon polycondensation/pyrolysis of $NH_4SCN$ and various heptazine derivatives.[9b,c] The as-obtained graphite-like "pseudo carbon nitrides" were classified according to their composition as "symmetric triangular forms" (cf. model **1c**, Scheme 1) or as partially condensed, irregular forms of heptazine-based polymers. In addition, the synthesis of a "cyameluric high polymer" by thermal de-ammonation of melon via a melem-dimer was postulated, affording a linear polymer composed of 42 monomers.[9d] In most cases, the X-ray powder patterns were indexed on orthorhombic unit cells ($a = 7.104$, $b = 16.190$, $c = 12.893$ Å;[9b] $a = 7.229$, $b = 21.512$, $c = 13.589$ Å).[9d] In contrast, the attempt to prepare carbon nitrides by polycondensation of melamine with the Lewis acid $ZnCl_2$ afforded a polymer with similar orthorhombic metrics, which was assigned a vacancy-network structure consisting of triazine cores.[9a]

As outlined above, the synthetic strategy that appears to be most promising to obtain reasonably well-defined carbon nitride materials includes the controlled pyrolysis of $CN_xH_y$ precursors.[15] However, the advantage of comparatively high crystallinity usually accompanies the presence of hydrogen in the products, which at the same time seems to stabilize the structure and to function as defect site. On the other end of the experimental spectrum, high-energy techniques (ion beam sputtering, CVD, laser- or shock-wave techniques) almost exclusively afford amorphous materials with substoichiometric nitrogen content with respect to the idealized formula $C_3N_4$.

  

In this work we present the 2D structure of a material, subject to numerous speculation, that has commonly been identified with graphitic carbon nitride. We thus provide the first structural characterization of a polymeric carbon(IV) nitride based on electron diffraction and solid-state NMR spectroscopy, which at the same time resolves the controversial identity of melon.

## Results and Discussion

**Synthesis and characterization**: A brownish polymer of the approximate composition $C_3N_{4.4}H_{1.8}$, (N: 61.2; C: 36.0; H: 1.8) determined from elemental analysis and with an average C/N ratio of 0.68 (theor. for $C_3N_4$: 0.75) was obtained by heating melamine (triamino-*s*-triazine) in sealed silica glass ampoules at 630 °C. Whereas at temperatures below 620 °C, melem ($C_6N_7(NH_2)_3$) was found in the products, thermolysis above 640 °C leads to rapidly increasing carbonization. It should be pointed out that heating melamine at 500 °C in an open system for several hours affords polymeric materials with different colors ranging from light yellow to dark beige. Whereas under these conditions, largely amorphous compounds are obtained, the crystallinity is significantly enhanced by pyrolyzing melamine in a closed system under an autogenous pressure of ammonia that arises from the condensation reactions. The brownish color of the as-obtained products suggests that crystallization accompanies the onset of carbonization of the sample. Small amounts of oxygen (up to 2 wt%; typically 0.5–0.7 wt%) detected in the bulk suggest that the material is prone to water absorption, as was pointed out in the literature.[17] In addition, melamine crystals were detected as impurities, which likely result from depolymerization of the product induced by ammonolysis at elevated temperatures and pressure of ammonia.[18] Possible depolymerization products other than melamine, such as dicyandiamide, were not observed as crystalline side phases; however, the presence of very small amounts of amorphous by-products such as (poly)imides below the detection level of solid-state NMR spectroscopy ($\leq$5% for CP measurements) may not entirely be excluded. Also, the comparatively harsh synthetic conditions applied in the present context likely induce heterogeneous crystallization and probably yield a broad spectrum of differently ordered domains, ranging from amorphous to nanocrystalline. Presumably, a mixture of polymers with different chain lengths is obtained, which can be considered a feature intrinsic to thermally induced polymerization processes. In this sense, the as-synthesized material, which will be referred to as "C/N/H-graphite" owing to its commonly inferred graphite-like character,[7] cannot be considered an overall homogeneous phase.

In situ temperature-programmed X-ray powder diffraction shows that the material is stable up to about 770 °C without passing through phase transitions prior to its decomposition. The observed thermal stability of this lightweight material is therefore comparable to or somewhat higher than that of aromatic polyamides and -imides.[9d]

The FTIR spectrum of C/N/H-graphite is displayed in Figure 1. Owing to obvious analogies with the vibrational spectra of melon already present in the literature,[9d,19] we will only focus on the most important results here. The well-

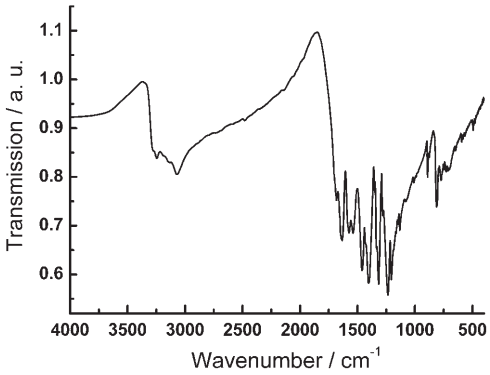


Figure 1. FTIR spectrum of melon recorded as a KBr pellet between 400 and 4000 $cm^{-1}$.

resolved bands indicate a fairly high degree of ordering. Whereas the sharp band at about 810 $cm^{-1}$ can be attributed to the ring-sextant out-of-plane bending vibration characteristic of both triazine or heptazine ring systems,[13,15,20] the prominent absorption bands at 1206 and 1235 $cm^{-1}$ and possibly 1316 $cm^{-1}$ have been shown to be characteristic of the C–NH–C unit in melam.[19,21,22] Therefore, a similar structural motif, corresponding to either trigonal C–N(-C)–C (full condensation) or bridging C–NH–C units (partial condensation), can be inferred for the polymer. Absorption found in the N–H stretching region between 3250 and 3070 $cm^{-1}$ proves the presence of NH and/or $NH_2$ groups, which are most likely integral parts of the structure.

Scanning electron microscopy images demonstrate the micro- and nanocrystalline character of the $CN_xH_y$ material as shown in Figure 2. The morphology of the material resembles that of microcapsules, the hollow tubes and spheres with a diameter of several micrometers containing nanocrystallites. While the crystalline particles appear to be platelike, the spheres presumably result from the isotropic bulging of the particles during gas evolution in the course of condensation. Owing to the small crystallite size, structure elucidation by X-ray methods does not seem to be particularly promising.

In accordance with literature data, the X-ray diffraction pattern is indicative of a layered substance with an interlayer spacing of 3.19 Å.[7,8,14,15,24] The powder pattern resembles that of graphite, which has an interlayer spacing slightly larger than that of the carbon nitride material (3.33 Å) as shown in Figure 3. Remarkably, the strong reflection, which is commonly indexed as 002 by analogy with graphite, is sharp, whereas all *hk*0 and *h*0*l* reflections—if present at all—are weak and broadened. In addition, asymmetric shapes of the reflections ("tailing" towards higher $2\theta$ values, as seen for the low-angle reflection at $2\theta \approx 12.6°$), are visible. These features could result from "streaking" along $c^*$ due to

  

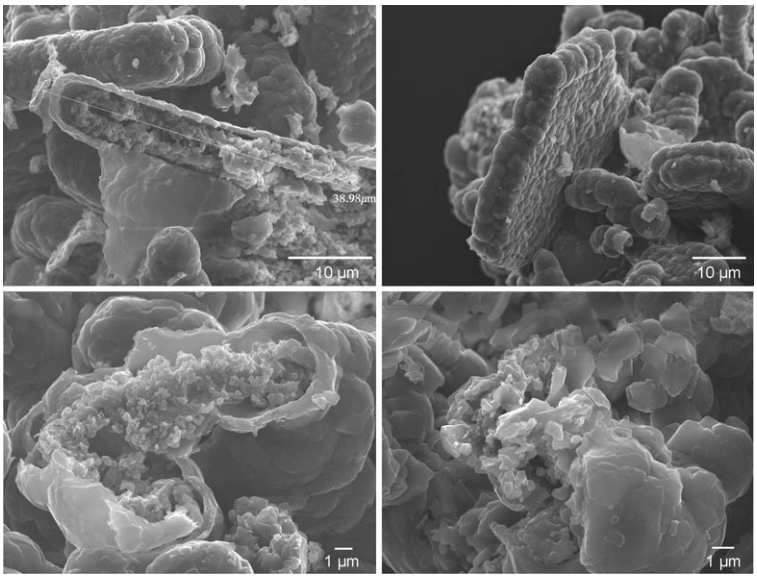


Figure 2. Scanning electron microscopy images of C/N/H-graphite, taken from various sample regions. The images reveal crystallite sizes on the nanometer- and micrometer-length scales, as well as the "porous" morphology of the sample.

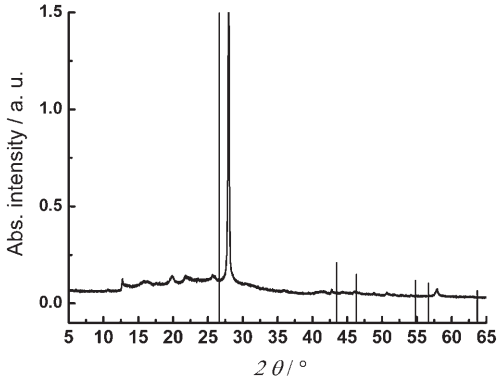


Figure 3. X-ray powder pattern ($Cu_{K\alpha 1}$ radiation) of C/N/H-graphite (continuous line) and simulation for graphite (bars). The interlayer distance (strong reflection) amounts to 3.19 Å.

2D planar disorder. However, the sharp main reflection and absence of splitting of the latter points to the layers being planar with a sharply defined interlayer spacing.

**Solid-state NMR spectroscopy**: Solid-state NMR spectroscopy is a valuable tool for probing the structure of semicrystalline or amorphous materials on local and intermediate length scales, as it is not dependent on the long-range order in contrast to diffraction techniques. Owing to the low sensitivity of the $^{15}N$ nucleus, a $^{15}N$-enriched C/N/H-graphite (degree of enrichment of $\approx 25\,\%$) was synthesized starting from $^{15}N$-labeled melamine.

The $^{15}N$ CP-MAS spectrum of the C/N/H-graphite is displayed in Figure 4 (top). The comparatively high resolution is diagnostic of a semicrystalline rather than an amorphous material. For a reliable signal assignment (as indicated in Figure 4), a CPPI (cross-polarization with polarization inversion) experiment was carried out. By evaluating the characteristic time dependence of the polarization inversion dynamics of the different $^{15}N$ nuclei, the number of protons covalently bonded to the latter can be ascertained. As outlined in Figure 5, three types of signals can be distinguished: The signals between $\delta = -177$ and $-195$ ppm, as well as the resonance at $\delta = -225$ ppm exhibit a moderate intensity loss, the continuous, slow decrease of the polarization being characteristic of tertiary nitrogen atoms. In contrast, the polarization of the signals at $\delta = -245$ and $-265$ ppm follows a two-step process induced by the covalently bonded protons. The intensity at the cross-over

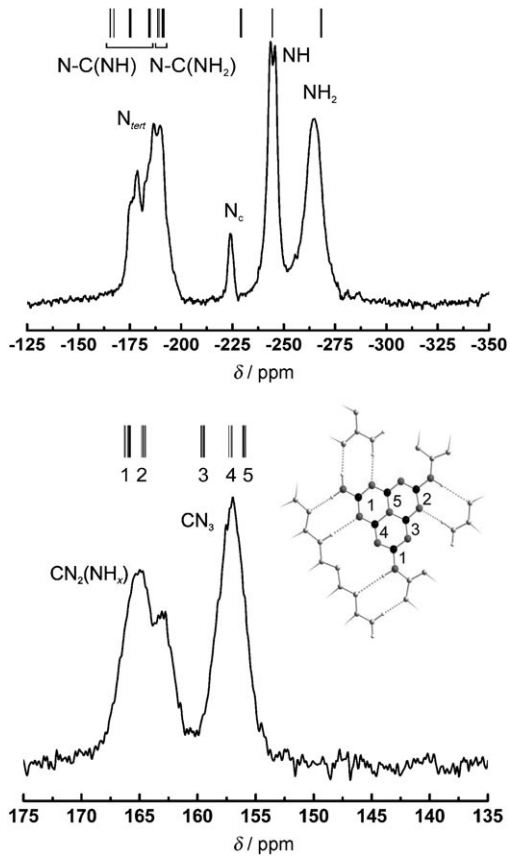


Figure 4. $^{15}N$ (top) and $^{13}C$ (bottom) CP-MAS solid-state NMR spectra of the C/N/H-graphite. The signal assignments according to ab initio calculations of the chemical shift values for the DFT-optimized cell (see inset) are indicated on top of the experimental spectra. The respective carbon sites in the structure are indicated by numbers (black: C, gray: N).

  

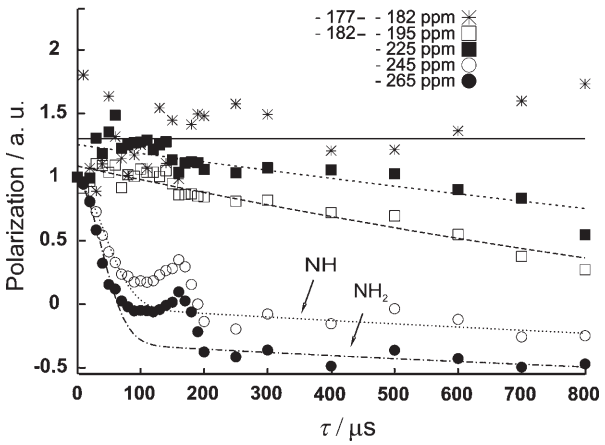


Figure 5. Evolution of the signal intensities (cf. Figure 4) during the course of a $^{15}N$ CPPI experiment. The polarization of the $^{15}N$ nuclei is given as a function of the inversion time $\tau_i$.

between the dipolar and spin-diffusion regime is given by $[2/(n+1)]-1$ ($n=0,1,2$), thereby allowing the differentiation between NH (crossover at 0) and $NH_2$ (crossover at $-1/3$) nitrogen nuclei.[13,25]

Therefore, the assignment of all signals according to the proton environment of the $^{15}N$ nuclei is feasible. Notably, apart from tertiary nitrogen atoms expected for a fully condensed network, NH and $NH_2$ groups are present, which suggest the formation of an only partially condensed C/N/H network.

Information on the nature of the building blocks can be obtained from the isolated signal at $\delta=-225$ ppm in the $^{15}N$ spectrum. This tertiary nitrogen resonance is strongly reminiscent of the central nitrogen atom ("$N_c$") of the heptazine core, since it exhibits an up-field shift compared to the outer nitrogen nuclei of the ring in essentially all heptazine-based compounds studied so far.[13,26] For example, this nitrogen resonance is observed at $\delta=-234.2$ ppm for melem.[13,24] Thus, these findings furnish the first significant indication of the heptazine-based nature of the graphitic C/N/H material.

The $^{13}C$ CP-MAS spectrum of the product shows remarkable similarity with that of melem. In detail, two signal groups are found with peak maxima at $\delta\approx164$ and 157 ppm. In melem, two groups of carbon resonances are observed at $\delta=164.3/166.4$ and 155.1/156.0 ppm, respectively, where the low-field signals ($\delta=164$–166 ppm) were assigned to the carbon positions adjacent to the amino groups.[13,24] Based on DFT calculations, an analogous assignment of the low-field signals ($\delta=163$–165 ppm) to $CN_2(NH_x)$ and the high-field signal ($\delta=157$ ppm) to $CN_3$ moieties was accomplished for the C/N/H-graphite as will be discussed below. The use of different CP contact times $\tau_c$ corroborates this assignment.

To quantify the relative $^{15}N$ signal intensities and to draw conclusions on the degree of condensation of the presumed heptazine core, an experiment using direct excitation of the $^{15}N$ nuclei was carried out (Figure 6). In this experiment, the magnetization transfer from the abundant protons to the $^{15}N$ nuclei is circumvented, thereby rendering the signal intensities independent of the number of protons in spatial proximity. Owing to the very long relaxation time of the $^{15}N$ nuclei, a recycle delay between successive scans of 8 h had to be applied to ensure total magnetization recovery before each scan. Comparatively long relaxation times are diagnostic of well-ordered materials. Owing to the isotopic enrichment of melon, 16 scans were sufficient to acquire a spectrum with a reasonable signal-to-noise ratio. As depicted in Figure 6, the signal intensities show significant variations as compared to the CP-MAS spectrum in Figure 4. As expected, the tertiary nitrogen resonances gained intensity at the expense of the protonated nitrogen signals. A quantitative fit of the relative intensities indicates a ratio of the four signal groups $N_{tert}$:$N_c$:NH:$NH_2$ roughly corresponding to 7:1:1:1. In particular, the equal intensities of $N_c$, NH, and $NH_2$ suggests a degree of condensation approximately corresponding to that expected for melon (6:1:1:1, cf. **1a** + **1b**, Scheme 1). To sum up, evidence of only one single type of building block—heptazine—is provided by the CP-MAS and direct excitation spectra. Since atom connectivities and, hence, local structural motifs dominate the chemical shift of the nuclei, this missing spread in chemical shift values renders the presence of triazine ring systems highly unlikely. In addition, DFT calculations of the chemical shift parameters of fully condensed triazine- and heptazine-based $C_3N_4$ systems suggest that the chemical shift range expected for triazine-based structures would spread out way downfield as compared to the observed data, for both planar and corrugated structures.[27] This adds to the above evidence that the C/N/H-graphite is composed of heptazine rather than triazine building blocks. Accordingly, the somewhat higher intensity observed for $N_{tert}$ may result from the admixture of minor, heptazine-based side phases exhibiting a slightly higher degree of condensation (cf. for instance structure **1c**, Scheme 1). The line width observed in the NMR spectra is slightly increased (by a factor of about 2) as compared to typical line widths of crystalline molecular compounds. This is indicative of varying chemical environments of the heptazine nuclei, which depend on the orientation of the adjacent layers as determined by the local stacking sequence. Similar

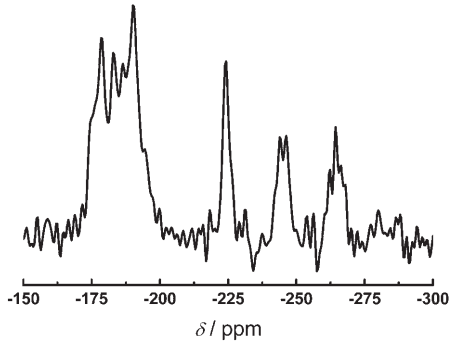


Figure 6. $^{15}N$ direct excitation spectrum using a recycle delay of 8 h as estimated from a $^{15}N$ $T_1$ measurement to ensure a total recovery of the magnetization. Number of scans: 16; spinning frequency: 9 kHz.

  

effects may be induced by different polymer lengths, which give rise to slightly altered local magnetic fields at the sites of nuclei in the vicinity of chain or layer terminations. In contrast, for a completely amorphous material the line widths should be increased by a factor of 10 to 20.

A fp-RFDR experiment was carried out to probe the homonuclear, through-space magnetization transfer between the $^{15}N$ nuclei. It can therefore be considered as a sensor for spatial proximities of the nuclei in the sample. By selectively exciting the $NH_2$ signal, the time dependence of the magnetization transfer to the surrounding $^{15}N$ nuclei (other than $NH_2$) was monitored by successively varying the mixing time in small intervals. Figure 7 (top spectra) outlines the

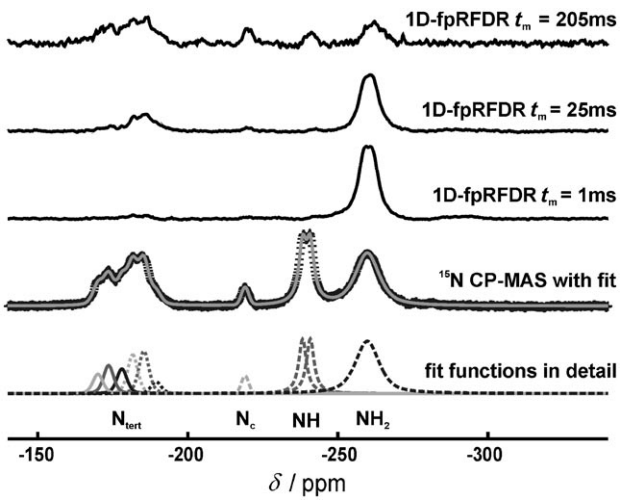


Figure 7. $^{15}N$ CP-MAS spectrum of the C/N/H-graphite and the corresponding overall fit (gray line; 2nd spectrum from bottom). Individual resonances of the fits (cf. Figure 8) (bottom), and 1D-fpRFDR spectra for mixing times $t_m = 1$, 25, 205 ms.

1D-RFDR spectra obtained for three mixing times ($t_m = 1$, 25, and 205 ms) corresponding to short, intermediate and long periods of magnetization transfer. Whereas for $t_m =$ 1 ms no magnetization transfer to the other nitrogen nuclei is visible, exchange commences at $t_m = 25$ ms for the high-field part of the tertiary nitrogen signals, which is visible by the growing intensity of the latter. Very weak signals can also be distinguished for the $N_c$ and NH resonances. For long mixing times, all initial resonances are observable, which indicates a dipolar exchange of magnetization among the $NH_2$ nitrogen and *all* other $^{15}N$ nuclei in the sample. This observation is confirmed by the build-up curves (see Figure S4 in the Supporting Information), which trace the increase of magnetization at the tertiary and NH nitrogen nuclei and the concomitant loss of signal intensity at the selectively excited $NH_2$ nitrogen atoms. Build-up is fastest for the tertiary $^{15}N$ nuclei from $\delta = -195$ to $-187$ ppm, which therefore represent the closest neighbors of the $NH_2$ group. This finding is in agreement with the ab initio $^{15}N$ chemical shift parameters calculated for the DFT-optimized cell based on the structure solution from electron diffraction, as will be detailed below (see also Figure 4). This exchange behavior suggests homogeneity of the sample in a regime up to 30 Å. Note that the coexistence of different domains is thus limited to different stacking variants and possibly heptazine-based structural isomers, which do not give rise to additional signals in the 1D CP-MAS spectrum as outlined above. Summing up, this experiment suggests that all $^{15}N$ nuclei are in spatial neighborhoods and no structurally distinct phases are detectable by $^{15}N$ NMR spectroscopy.

**Electron diffraction**: Electron diffraction (ED) can provide structural insights into nanometer-sized materials. The dimensions of the C/N/H-graphite particles can be estimated to amount to 50–200 nm by transmission electron microscopy (TEM, Figure 8). In the diffraction mode, the presence of domains (Figure 9) of varying crystallinity is evident, as can

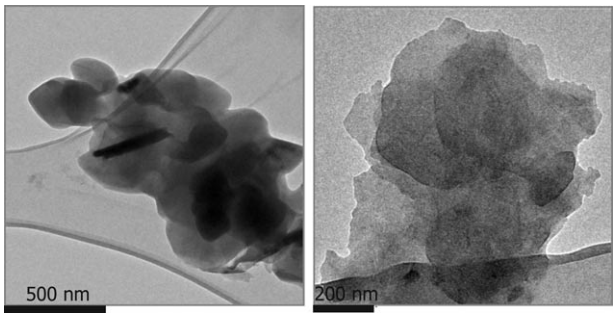


Figure 8. TEM images of the C/N/H-graphite on a carbon coated copper grid, showing the platelike nano- and microcrystals.

be seen by the asymmetric peak shapes and diffuse scattering, the latter being either intrinsic or due to amorphous cover layers. In agreement with the platelike character of the crystallites, the preferred orientation is such that most diffraction patterns are taken along the [001] zone axis, other zone axes are hardly accessible. As indicated by the X-ray powder patterns, varying degrees of "streaking" along $c^*$ are observable (Figure 10, right), resulting from planar defects or possibly turbostratic stacking disorder. Nevertheless, SAED patterns of crystalline domains with perfect pe-

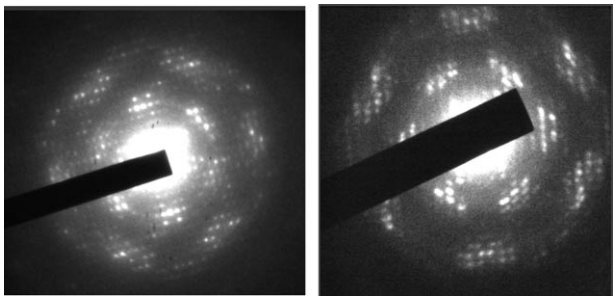

Figure 9. Selected area electron diffraction (SAED) patterns of the *hk*0 plane (zone axis [001]) of the C/N/H-graphite. All patterns exhibit different degrees of diffuse scattering and are indicative of partial disorder and/or thick sample sizes.

  

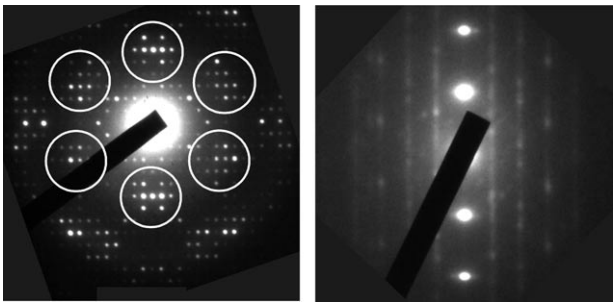

Figure 10. Left: Electron diffraction pattern of the *hk*0 plane (zone axis [001]). The pseudo-hexagonal intensity distribution is indicated by white circles. Merging the reflection groups contained in the circles (shown exemplarily; the same applies for all reflection groups) into one single spot would generate a diffraction image similar to that of graphite. Right: SAED pattern viewed perpendicular *c**. Whereas the 00*l* reflections are clearly visible, "diffuse bars" are observed parallel to *c** with a non-discrete intensity distribution ("streaking").

riodicity at least in two dimensions can be obtained, which are unaffected by the stacking disorder (Figure 10, left).

The commonly claimed graphite-like character of this material, which has led to the assumption that it is related to graphitic carbon nitride, is associated with the pseudo-hexagonal intensity distribution in the *hk*0 plane. Groups of strong reflections can be correlated with reflections of graphite with respect to their symmetry as well as the encoded distance information (Figure 10, left). Indexing the *hk*0 patterns yields a rectangular mesh with cell parameters $a=16.7$, $b=12.4$ Å. These values are similar to those determined by Komatsu from X-ray powder patterns ($a=7.104$ ($\equiv$ 2c), $b=16.190$ ($\equiv$ a), $c=12.893$ Å ($\equiv$ b)) given the layer spacing of 3.2 Å.[9b] Taking advantage of a number of beneficial factors, such as the planarity of the layers, the light atom structure, and large unit cell (small structure factors, minimum multiple scattering), the structure was solved in projection based on the electron diffraction data. Owing to the small sample thickness, the kinematical approximation $I_{hkl} \propto |F_{hkl}|^2$ could be used. Evaluation of the observed absences in the base plane (*h*0: $h=2n+1$; 0*k*: $k=2n+1$) allows for the plane group *p*2*gg*. Strong reflections remain sufficiently strong to find phase relationships using direct methods,[28a] and, thus, a figure of merit of 20.06% was obtained by employing SIR-97[29] for structure solution. Reducing the symmetry to *p*2 and introducing the mirror planes as a twin law yields better residuals. However, the data/parameter ratio obtained is very low. Therefore, the improvement of the residuals is not significant and is accompanied by an unreasonable distortion of the heptazine rings. Upon regularizing the heptazine units, the residuals again increase, so that the twin approach does not lead to a real improvement.

All carbon and nitrogen atoms could be located with reasonable bond angles and distances. Upon refinement (208 reflections, 46 parameters), *R*1 was 26.44%. As reflection intensities are affected by dynamical diffraction, better residuals have not been obtained; however, they lie in the range usually reported for refinements based on electron diffraction data.[28] After refinement, the difference Fourier synthesis has no significant maxima, which can be demonstrated by arbitrarily removing one atom from the structure model. The removed atom then yields by far the highest difference Fourier peak. The bond length precision after refinement is 0.045 Å, within this experimental error (neglecting systematic errors), the distances and angles calculated are reasonable within a 2σ interval. Crystallographic data are summarized in Table 1.[31]

Table 1. Crystallographic data of the structure solution and refinement of melon based on ED data.

| | |
|---|---|
| formula | $C_6N_9H_3$ |
| $M_w$ [g mol$^{-1}$] | 201 |
| plane group | *p*2*gg* |
| instrument type | JEOL 2011 TEM |
| instrument details | single tilt holder, TVIPS CCD camera (F114) |
| incident radiation energy [kV] | 200 |
| $d_{min}$ [Å] | 0.65 |
| *a* [Å] | 16.7[a] |
| *b* [Å] | 12.4[a] |
| layer distance along *c* [Å] | 3.2[b] |
| symmetry-independent reflections | 208 |
| number of parameters | 46 |
| *R*1 | 26.44% |
| $R_{rim}$[29] | 40.2% |

[a] The error for determination of the lattice parameters from ED is estimated to be $\approx$5%. [b] Determined from X-ray powder diffraction.

To countercheck the consistency of the structure model, kinematical SAED diffraction patterns based on the structural parameters were calculated. The simulation of the *hk*0 plane is shown in Figure 11 (right), together with experimental patterns used for structure solution. The patterns agree well, although the experimental intensity distribution deviates slightly from the *mm*2 symmetry of the plane group. Note however, that the symmetry of the precession patterns is significantly less violated.

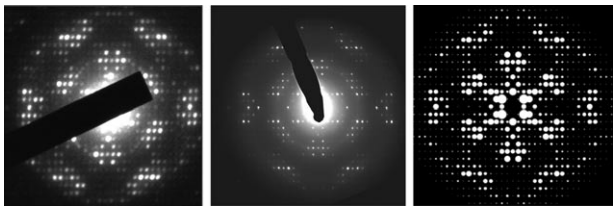

Figure 11. Experimental (left, middle) *hk*0 diffraction patterns, from which the structure solution in projection was accomplished. The left diffraction pattern was recorded under "static" conditions and its intensities merged with a second pattern (not shown); the middle pattern was recorded by using the precession technique.[27g,30] Right: Simulation of an SAED pattern of the 0th layer based on the proposed structural model, assuming ideal kinematical scattering of electrons.

The 2D projection of the crystal structure is displayed in Figure 12. The layers comprise infinite chains of "melem-monomers" condensed via N(H) bridges, thereby forming a

  

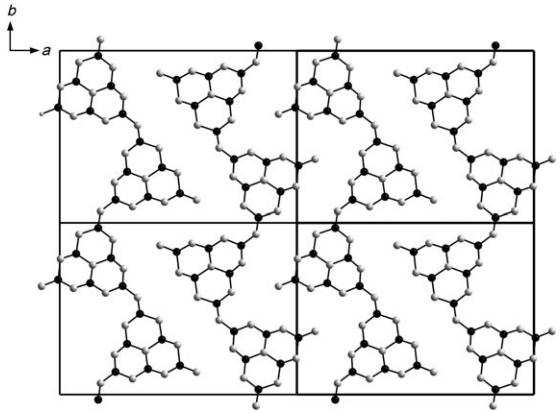


Figure 12. Projection of the structure of melon. Hydrogen atoms and molecular fragments from adjacent strands are omitted for clarity; black: C, gray: N.

closely packed two-dimensional array. The heptazine strands are arranged in a zigzag-type fashion, allowing close N···N contacts of 3.1–3.4 Å between adjacent strands, which are bridged by medium strong hydrogen bonds between the ring-nitrogen atoms and the NH and $NH_2$ groups, respectively. Covalent interactions within the heptazine backbone and formation of a delocalized π system seem to play a pivotal role in fixing the planar geometry of the strands. Van der Waals-type interactions between the layers are likely to contribute significantly to the overall stabilization of the system; however, they appear to be largely unselective toward a particular kind of stacking sequence.

As the structure is built up from infinite 1D chains instead of 2D atomic arrays it does not represent any structure model postulated for hypothetical g-$C_3N_4$. In contrast, it corresponds to the "polymer" structure model proposed for melon (**1b**, Scheme 1),[3,4,9b] whose existence has therefore been substantiated. Detailed statements on the structure of the melon strands are now possible, as for instance the zigzag-type arrangement of the heptazine motifs as well as the close packing of the chains leading to a tightly hydrogen-bonded 2D array. Furthermore, the alternative structure model postulated for melon, which is based on a triangular-shaped trimer of melem (**1a**, Scheme 1), can be discarded at least in the present case. However, this does not in principle disavow the existence of this structural isomer of melon.

The structure solution presented above allows the unique determination of the 2D structure of melon, and is in full agreement with the spectroscopic data presented above. However, the stacking disorder of the bulk sample seems to impede a comprehensive 3D approach, as due to the disorder it may not seem straightforward that the projection yields the structure of a single layer. Nevertheless, possible interpretations of the structure projection will be delineated in the following.

As a starting basis, we assume that the 2D projection delineated above is only compatible with some sort of AAA… type stacking. Given the fact that X-ray powder patterns, theoretical calculations (see below), and the expected planarity of heptazine cores and amide/imide moieties[7a–c,8,14] indicate overall planarity of the layers, the maximum symmetry of a 3D structure in the case of eclipsed layers is given by space group *Pbam*. However, theoretical calculations (see below) suggest a lateral displacement of adjacent layers to be far more likely. These displacements become favorable, since π-stacking interactions usually require a slight displacement of adjacent layers to prevent repulsion of the negatively polarized π orbitals.[32] The above requirements can be met by considering layer-offsets in which *p*2*gg* symmetry is retained in the projections. In other words, it is reasonable to assume monoclinic 3D symmetry, which implies that the layers are laterally shifted along either *a* or *b* with a monoclinic angle $\neq$ 90° and an AAA… type of stacking. When viewed along [001], the associated diffraction patterns are very similar to those obtained for an orthorhombic setting. Therefore, the structure can alternatively be solved in the $P2_1/a$ space group (cell setting $a = 12.4$, $b = 16.7$ Å, $\beta$ between 92 and 115°, layers shifted along the *a* axis). Note that a layer offset along the *b* axis has the same negligible effect on the structure solution. Apart from slight distortions of the heptazine building blocks for $\beta \neq 90°$, the structure projection of eclipsed layers using orthorhombic and monoclinic variants, respectively, are hardly distinguishable. Other ordered models, such as those with an ABA… layer sequence, are incompatible with the experimental data; however, alternative explanations might be considered.

It seems unlikely that the thickness of the sample corresponds to only a few layers, which would yield 2D scattering and lead to an interpretation of the diffraction pattern in terms of a section through diffuse streaks along *c**. However, in the case of statistically shifted (but not rotated) layers, without any periodicity of the stacking sequence (cf. powder diagram, Figure 3), the *z* component of Patterson vectors is lost, and the *hk*0 section would be likewise representative of interatomic distances only perpendicular to *c*. In other words, a structure determination would yield the structure of a single layer. Diffraction patterns like that shown in Figure 10 (right) might corroborate this situation;[33] however, it is impossible to ascertain the exact zone axis orientation. Therefore, we can conclude that the true situation is to be found between the borderline cases outlined here.

**Theoretical calculations**: Theoretical calculations were used as an independent verification of the structure model obtained from electron diffraction. To this end, complementary calculations were carried out based on three different computational methods. Both a single chain comprising nine heptazine molecules, as well as an array of six chains containing six heptazine monomers each were optimized by using the PM3 method.[34,35]

Energy minimization reveals that the single zigzag chain as found by ED already possesses a stable molecular arrangement in the gas phase. Its geometry after optimization is outlined in Figure 13 (right). As an alternative, the classically proposed straight melon chain bends upon energy minimization as demonstrated in Figure 13 (left). The tendency

  

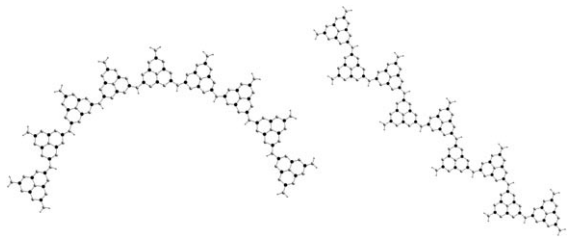

Figure 13. PM3-optimized polymeric models of melon. Left: "Classical" model of an initially linear (starting geometry) melon chain with identical alignment of the heptazine monomers. The linear chain bends upon energy minimization. Right: Zigzag chain of melon as obtained from ED. Gray: N; black: C; gray: H; the positions of the latter are empirically fitted.

of a pair of NH-bridged heptazine rings to bend apart is also visible in the linear zigzag arrangement, whereby the alternating curvatures about every NH bridge compensate, yielding an overall linear array. When assembling six zigzag chains into a 2D arrangement according to the structure proposed by ED, a planar oligomer is obtained upon optimization, which is highly stabilized by a tight hydrogen-bonding network (compare Figure 14).

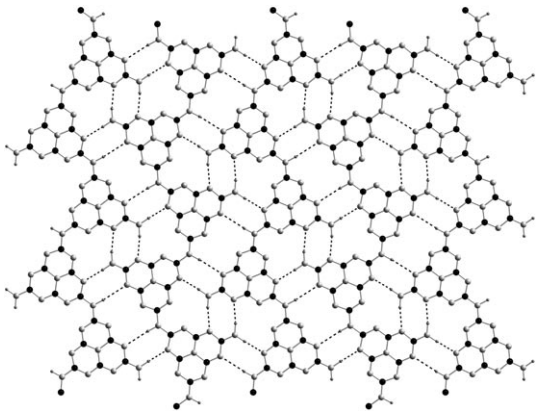

Figure 14. Planar cluster of melon after geometry optimization under periodic boundary conditions using CASTEP. The hydrogen positions are empirically fitted and the hydrogen-bonding network is indicated by black dots. Gray: N; black: C; gray: H.

To calculate the NMR chemical shift parameters for a single layer of melon, the latter was further optimized by using DFT (Figure 14).[36] The periodicity of the PM3-optimized core region of the above planar oligomer allowed the extraction of the *a*/*b* cell parameters and the establishment of a rectangular unit mesh. Although symmetry restrictions were not applied during structure optimization, a planar structure with a rectangular mesh was retained. Whereas the resulting *b* axis matches the value found by calculations at the PM3 level, the *a* axis is slightly elongated as outlined in Table 2. The overestimation of the *a* axis can be rationalized by the poor description of dispersion forces in hydrogen-bonding networks obtained by using DFT. Furthermore, attempts to optimize an orthorhombic unit cell with an interlayer spacing of 3.2 Å does not lead to a minimum on the energy surface. This renders orthorhombic metrics associated with an AAA… stacking extremely unlikely.

Table 2. Experimental and calculated lattice parameters for the structure of melon obtained from ED and different theoretical approaches.

| Method | *a* [Å] | *b* [Å] | Interlayer distance [Å] |
|---|---|---|---|
| CASTEP[a] | 17.1 | 12.8 | (4.43)[a] |
| PM3[b] | 16.6 | 12.7 | |
| DREIDING | 16.7–16.8 | 12.8 | 3.2–3.4 |
| TEM/XRD | 16.7[c] | 12.4[c] | 3.2[d] |

[a] Constrained during geometry optimization. [b] Cluster of 36 hepatazine units arranged in six planar zigzag chains. [c] Estimated error ≈5%. [d] X-ray powder diffraction.

An overall description including dispersion interactions between individual layers is possible based on force field methods.[37,38] The *a* and *b* axes are in excellent agreement with the values calculated by using PM3 and CASTEP (Table 2). For an eclipsed layer arrangement, which is considered to be energetically unfavorable in terms of interlayer van der Waals interactions, the repulsive inter-planar forces are maximized, and a layer distance of 3.4 Å is obtained. In contrast, for layer arrangements exhibiting an offset stacking—not complying with orthorhombic metrics—cells with interlayer distances of 3.2 Å were found, as observed in the experiment.

For the DFT-optimized unit mesh, ab initio $^{13}C$ and $^{15}N$ NMR chemical shift parameters were calculated. As demonstrated in Figure 4, the calculated $^{13}C$ and $^{15}N$ chemical shifts are in good agreement with those in experimental spectra and confirm the overall signal assignments extracted from the CPPI experiment. The $^{13}C$ chemical shift range is reproduced by the calculations; in the theoretical $^{15}N$ spectrum, the resonance of the central nitrogen atom is slightly shifted towards higher field; the same tendency is observed for the NH and $NH_2$ groups. The calculated chemical shifts also allow one to distinguish between tertiary nitrogen atoms bonded to different $NH_x$ groups, since they are directly affected by the surrounding NH (low-field shift) and $NH_2$ moieties (high-field shift), respectively. These observations match well with the results from the 1D fp-RFDR NMR experiment and confirm the structure model derived from the ED experiments.

## Conclusion

The above results shed light on the long-standing debate concerning the identity of Liebig's inert compound "melon", whose structure has now been proven for the first time. The 2D structure of melon reveals the heptazine molecular building blocks and polymeric nature of this important $CN_x$ precursor. Owing to the weak attractive interlayer forces, the "bulk" 3D structure is intrinsically affected by inherent planar defects associated with translations of the layers. Different energetically similar stacking modes with various translational layer offsets are likely to contribute to the

  

overall 3D structure.[39] This feature adds to the special importance of understanding the 2D arrangement of the molecular building blocks.

Considering the fact that melon is composed of planar layers built up by a carbon(IV) nitride core (heptazine units), this compound may be considered as a "defective g-$C_3N_4$" material, whose graphite-like topology may in fact result from the presence of network terminations in the form of NH and $NH_2$ groups. These function as triggers for strain release in such a way that buckling of the sheets is prevented. As has recently been noted,[14b] melon (in that work called g-$C_3N_4$) may therefore be considered a promising functional material in catalysis or surface science, and at the same time represent a pre-stage of graphitic carbon nitride. Along the same lines, the recently synthesized $sp^3$-hybridized carbon nitride imide $C_2N_2(NH)$, which represents a formal pre-stage of 3D $C_3N_4$, can be considered the high-pressure analogue of melon.[40]

However, the existence of melon highlights characteristic differences between graphite and "graphitic" carbon nitride materials, and in doing so, demonstrates that the analogy between the two systems is clearly limited both with respect to chemical and structural aspects. Given the fact that essentially all attempts to prepare g-$C_3N_4$ from hydrogen-containing precursors yield materials with similar structural features and hydrogen contents, we hypothesize that the products of the frequently claimed syntheses of graphitic carbon nitride have in fact rather been polymers such as melon or related compounds.[7,14,11,9a–c] We can thus add the first direct evidence to the ongoing debate on the structure of the hypothetical g-$C_3N_4$, that triazine-based models, which are still predominantly being discussed in the literature, should henceforward be assessed very critically. Therefore, the present work may stimulate a careful re-evaluation of commonly accepted paradigms about the existence and structure of graphitic carbon nitride.

## Experimental Section

**Synthesis of melon**: Pyrolyses of melamine were carried out in sealed silica glass ampoules under vacuum at temperatures between 560 and 600 °C, or predominantly under dry argon at temperatures between 620 and 640 °C. Typically, melamine (230 mg, $1.83\times10^{-3}$ mol; ≥ 99 %, Fluka) was transferred into a thick-walled silica glass tube ($\varnothing_{ext.}$ 15 mm, $\varnothing_{int.}$ 11 mm), from which water had been removed by thorough heating and evacuation. The tube was sealed by using a hydrogen burner at a length of about 120 mm. The ampoule was then placed in a vertical tube furnace and heated (1 K min$^{-1}$) to 630 °C, at which temperature the sample was held for 12 to 36 h. The cooling rates did not notably affect the crystallinity of the products, so that the furnace was typically switched off and the sample was allowed to cool down to room temperature over several hours. The sample was then isolated by carefully breaking the ampoule, upon which a significant amount of HCN and ammonia was released. The yield of brownish residue typically amounted to 38–57 %; approximately 8–10 % were recovered from the top of the ampoule in the form of a brown sublimate mixed together with long, needle-shaped melamine crystals. To purify the residue and eliminate melamine and—present to only a small extent—melem crystals, the product (≈80–100 mg) was transferred into a Duran ampoule (pre-dried in vacuo under heating), which was sealed off under an atmosphere of argon and heated to temperatures around 600 °C (1 K min$^{-1}$) for at least 12 h. Alternatively, admixtures of the starting material melamine were removed by sublimation using a cold finger integrated into a glass tube. Upon purification, the brownish material lightened up, thereby changing its color into reddish-brown.

$^{15}$N-enriched melamine was prepared according to the procedure introduced by Jürgens et al.[13,24] Sodium tricyanomelaminate $Na_3[C_6N_9]$ was prepared by heating sodium dicyanamide $Na[N(CN)_2]$ (2 g; ≥ 96 %, Fluka) to 500 °C (5 K min$^{-1}$) in a quartz tube under pressure equalization and subsequently reacting the as-obtained material (742.5 mg, $2.78\ 10^{-3}$ mol) with $^{15}NH_4Cl$ (183 mg, $3.36\times10^{-3}$ mol, ≥ 98 %, Cambridge Isotopes) in a Duran tube (length: 160 mm, $\varnothing_{ext.}$: 26 mm, $\varnothing_{int.}$: 24 mm) at 470 °C (1 K min$^{-1}$) for 12 h.[13,24] The raw material was further purified by sublimation (1 Pa, 220 °C).

**General techniques**: Elemental analyses were performed by using a commercial C, H, N elemental analyzer system Vario EL (Elementar Analysensysteme GmbH).

XRD measurements were performed on a Stoe-Stadi P diffractometer. High-temperature in situ X-ray diffraction was carried out on a STOE Stadi P powder diffractometer (Ge(111)-monochromated $Mo_{K\alpha1}$ radiation, $\lambda = 70.093$ pm) with an integrated furnace using unsealed quartz capillaries ($\varnothing$ 0.5 mm) as sample containers.

FTIR measurements were carried out on a Bruker IFS 66v/S spectrometer. Spectra of the samples were recorded by utilizing KBr pellets (1 mg sample, 500 mg KBr, hand press with press capacity 10 kN) in an evacuated cell equipped with a DLATGS detector at ambient conditions between 400 and 4000 cm$^{-1}$.

Scanning electron microscopy was performed on a JEOL JSM-6500F equipped with a field emission gun at an acceleration voltage of 10 kV. Samples were prepared by putting the powder specimen on adhesive conductive pads and subsequently coating them with a thin conductive carbon film.

**Solid-state NMR spectroscopy**: $^{13}$C and $^{15}$N CP-MAS solid-state NMR spectra were recorded at ambient temperature on the conventional impulse spectrometers DSX Avance 500 (Bruker) and DSX Avance 400 (Bruker) operating at a proton resonance frequency of 500 MHz and 400 MHz, respectively. The samples were contained in 4-mm $ZrO_2$ rotors, which were mounted in standard double-resonance MAS probes (Bruker). The $^{13}$C and $^{15}$N signals were referenced with respect to TMS and nitromethane, respectively. Data collection of all experiments was performed applying broadband proton decoupling using a TPPM sequence.[41] For the CP MAS spectra of both nuclei a ramped cross-polarization sequence was employed where the $^1$H pulse amplitude was decreased linearly by 50 %. Contact times between 10 ms and 20 ms were used and the recycle delay was chosen to allow a nearly complete magnetization recovery optimized via $^1$H spin-lattice relaxation experiments. The spinning frequencies $\nu_{rot}$ varied between 7 and 12 kHz. To determine the number of covalently bonded protons to the nitrogen atoms, a $^{15}$N CPPI[25] (cross-polarization combined with polarization inversion) experiment was performed ($\nu_{rot} = 6$ kHz). The polarization inversion behavior was probed by varying the inversion time from 0.2 to 800 μs (28 spectra), with an initial contact time of 2 ms. $^{15}$N direct excitation spectra were acquired with three back-to-back 90° pulses to eliminate unwanted contributions from the probe and ringing effects.[42] The nutation frequency and the recycle delay were adjusted to 75 kHz and 28800 s (= 8 h) (estimated from a $^{15}$N $T_1$ measurement) to ensure a total recovery of the magnetization. A total amount of 16 scans was collected and the spinning frequency was set to 9 kHz. To probe homonuclear $^{15}$N connectivities and distances, selective excitation fp-RFDR experiments were performed by using a XY-16 phase cycle.[42] For the fp-RFDR mixing block active rotor synchronization was applied with $\nu_{rot} = 15$ kHz. The length of the soft 180° pulse in the middle of each rotor period was adjusted according to $p(180°) = 0.3\cdot1/\nu_{rot}$ corresponding to a nutation frequency of 25 kHz. To ensure a selective excitation of the $^{15}$N resonance of the $NH_2$ groups a CP sequence with a short CP contact time (90 μs) was followed by a comb of two 90° pulses (3.4 μs) on-resonant on the $NH_2$-signal with an interpulse spacing $\tau$ between 280 μs and 340 μs corresponding to $\tau =$

  

$^1/_4(\nu(NH)-\nu(NH_2))^{-1}$. The short contact time excites only NH and $NH_2$ resonances significantly. Afterwards the comb of 90° pulses allows one to dephase the magnetization of the off-resonant resonance while preserving the magnetization of the on-resonant one.

**Electron diffraction/transmission electron microscopy**: ED and TEM measurements were carried out on a JEOL 2011 instrument equipped with a tungsten cathode operating at 200 kV. The images were recorded using a TVIPS CCD camera (F114). The sample was finely dispersed by sonication in ethyl alcohol suspension for 30 minutes, and a small amount of the suspension was subsequently dispersed on a copper grid coated with holey carbon film. The grids were mounted on a single tilt holder with a maximum tilt angle of 30° and subsequently transferred to the microscope. Suitable crystallites were singled out among those yielding diffraction patterns of main poles, typically with the zone axis [001] aligned along the electron beam. The selected-area aperture was adapted in each case to the size of the selected thin crystalline domains. Precession experiments were conducted by using a FEI Tecnai 12 transmission electron microscope with a $LaB_6$ cathode, operating at 120 kV and equipped with a Spinning Star precession interface (NanoMEGAS). A precession angle of approximately 1.5° was applied. The images were recorded on a TVIPS 2k CCD camera (F224HD) with a dynamic range exceeding 25000:1. Reflection intensities were extracted by using the ELD program package;[44] for simulation of the kinematical diffraction patterns the program JSV1.08 Lite[45] was employed. Calculation of the electron diffraction patterns was done using the programs VEC[46] and JEMS.[47] In principle, it is possible to solve a structure provided the strong reflections remain sufficiently strong to find phase relationships using direct methods.[28a] To quantify all strong *hk*0 reflections, intensities of two *hk*0 diffraction patterns were merged, yielding a dataset of 208 independent reflections. Evaluation of the observed absences in the base plane (*h*0: $h=2n+1$; 0*k*: $k=2n+1$) indicates the presence of the plane group *p*2*gg*. Owing to the lack of detailed three-dimensional information, the structure was solved by using the space groups $P2_12_12$ or *Pbam*, which correspond to the plane group *p*2*gg* in (001) projection. The most probable solution as found by SIR-97[29a] had a figure of merit of 20.06 %.[29b] The heptazine molecular unit was obtained without prior fixation of parameters. Refinement of the ED data for calculation of Fourier maps was done with the program SHELX-97,[48] using the electron form factors as given by Doyle and Turner.[49]

**Calculations**: In the cluster approach the semiempirical PM3 method[34] was used for structure optimization with the Gaussian03 program package.[35] The input structures were created from the ED structure solution with hydrogen added to the NH and $NH_2$ groups. DFT calculations under periodic boundary conditions were performed with the MS Modelling 4.0 package by Accelrys. The input cell was created in orthorhombic symmetry from a cutout in the core region of the PM3-optimized structure. For the CASTEP[36] calculations the PBE functional and ultrasoft pseudopotentials were taken with sampling over 6 k-points. In the structure optimization of the input cell an energy cutoff of 280 eV was used. To ensure that the dispersion interaction between neighboring layers become negligible, a constrained slab of 4.43 Å along the *c* axis was introduced. NMR parameters were calculated with a cutoff of 350 eV for the optimized cell. For a core cutout of the PM3-optimized cluster the Hirschfeld charges were determined with the $DMol^3$ program, the PBE functional and the DNP basis set.[38] These partial charges were used in flexible body structure optimizations of the input cell with the Dreiding force field.[37] By default, 1,4-intramolecular electrostatic interactions were excluded from the energy evaluation.

## Acknowledgements

We gratefully acknowledge financial support that was granted from the Deutsche Forschungsgemeinschaft (DFG) (projects SCHN 377/12–1 and SE 1417/2–1), Fonds der Chemischen Industrie (FCI), the BMBF, and the Studienstiftung des Deutschen Volkes (scholarships for B. V. Lotsch). We gratefully acknowledge NanoMEGAS and TVIPS for providing us with their equipment and for experimental support to obtain the precession pattern, especially I. Daberkow and J. Portillo. We also thank Prof. E. Rössler (University of Bayreuth) for making available his NMR equipment, and Mrs. C. Buhtz for her support with the data analysis.

[1] a) M. L. Cohen, *Phys. Rev. B* **1985**, *32*, 7988; b) A. Y. Liu, M. L. Cohen, *Science* **1989**, *245*, 841; c) C.-M. Sung, M. Sung, *Mater. Chem. Phys.* **1996**, *43*, 1; d) D. M. Teter, R. J. Hemley, *Science* **1996**, *271*, 53.
[2] J. Liebig, *Ann. Pharm.* **1834**, *10*, 10.
[3] E. C. Franklin, *J. Am. Chem. Soc.* **1922**, *44*, 486.
[4] a) C. E. Redemann, H. J. Lucas, *J. Am. Chem. Soc.* **1940**, *62*, 842; b) L. Pauling, J. H. Sturdivant, *Proc. Natl. Acad. Sci. USA* **1937**, *23*, 615.
[5] B. Bann, S. A. Miller, *Chem. Rev.* **1958**, *58*, 131.
[6] a) L. Costa, G. Camino, G. Martinasso, *Polym. Prepr. Am. Chem. Soc. Div. Polym. Chem.* **1989**, *30*, 531; b) H. May, *J. Appl. Chem.* **1959**, *9*, 340.
[7] a) I. Alves, G. Demazeau, B. Tanguy, F. Weill, *Solid State Commun.* **1999**, *109*, 697; b) Kawaguchi, K. Nozaki, *Chem. Mater.* **1995**, *7*, 257; c) E. G. Gillan, *Chem. Mater.* **2000**, *12*, 3906; d) Q. Guo, Y. Xie, X. Wang, S. Lv, T. Hou, X. Liu, *Chem. Phys. Lett.* **2003**, *380*, 84; e) J. L. Zimmermann, R. Williams, N. Khabashesku, J. L. Margrave, *Nano Lett.* **2001**, *1*, 731; f) M. Todd, J. Kouvetakis, T. L. Groy, D. Chandrasekhar, D. J. Smith, P. W. Deal, *Chem. Mater.* **1995**, *7*, 1422; g) H. Montigaud, B. Tanguy, G. Demazeau, I. Alves, S. Courjault, *J. Mater. Sci.* **2000**, *35*, 2547; h) V. N. Khabashesku, J. L. Zimmerman, J. L. Margrave, *Chem. Mater.* **2000**, *12*, 3264; i) J. Kouvetakis, A. Bandari, M. Todd, B. Wilkens, *Chem. Mater.* **1994**, *6*, 811; j) D. R. Miller, D. C. Swenson, E. G. Gillan, *J. Am. Chem. Soc.* **2004**, *126*, 5372; k) D. R. Miller, J. Wang, E. G. Gillan, *J. Mater. Chem.* **2002**, *12*, 2463; l) S. Courjault, B. Tanguy, G. Demazeau, *C. R. Acad. Sci. Ser. IIc: Chim.* **1999**, *2*, 487; m) Z. H. Zhang, K. Leinenweber, M. Bauer, L. A. J. Garvie, P. F. McMillan, G. H. Wolf, *J. Am. Chem. Soc.* **2001**, *123*, 7788; n) Q. Guo, Y. Xie, X. J. Wang, S. Zhang, T. Hou, S. Lv, *Chem. Commun.* **2004**, *1*, 26; o) H. Montigaud, B. Tanguy, G. Demazeau, I. Alves, M. Birot, J. Dunogues, *Diamond Relat. Mater.* **1999**, *8*, 1707.
[8] a) E. Kroke, M. Schwarz, *Coord. Chem. Rev.* **2004**, *248*, 493; b) S. Muhl, J. M. Mendez, *Diamond Relat. Mater.* **1999**, *8*, 1809; c) T. Malkow, *Mater. Sci. Eng. A* **2001**, *302*, 311; d) M. C. dos Santos, F. Alvarez, *Phys. Rev. B* **1998**, *58*, 13 918.
[9] a) T. Komatsu, *J. Mater. Chem.* **2001**, *11*, 799; b) T. Komatsu, *J. Mater. Chem.* **2001**, *11*, 802; c) T. Komatsu, T. Nakamura, *J. Mater. Chem.* **2001**, *11*, 474; d) T. Komatsu, *Macromol. Chem. Phys.* **2001**, *202*, 19.
[10] D. T. Vodak, K. Kim, L. Iordanidis, P. G. Rasmussen, A. J. Matzger, O. M. Yaghi, *Chem. Eur. J.* **2003**, *9*, 4197.
[11] G. Demazeau, *J. Mater. Chem.* **1999**, *9*, 15.
[12] E. Kroke, M. Schwarz, E. Horath-Bordon, P. Kroll, B. Noll, A. D. Norman, *New J. Chem.* **2002**, *26*, 508.
[13] B. Jürgens, E. Irran, J. Senker, P. Kroll, H. Müller, W. Schnick, *J. Am. Chem. Soc.* **2003**, *125*, 10 288.
[14] a) M. Groenewolt, M. Antonietti, *Adv. Mater.* **2005**, *17*, 1789; b) F. Goettmann, A. Fischer, M. Antonietti, A. Thomas, *Angew. Chem.* **2006**, *118*, 4579; *Angew. Chem. Int. Ed.* **2006**, *45*, 4467.
[15] a) B. V. Lotsch, W. Schnick, *Chem. Mater.* **2005**, *17*, 3976; b) B. V. Lotsch, W. Schnick, *Chem. Mater.* **2006**, *18*, 1891.
[16] a) R. S. Hosmane, M. A. Rossman, N. J. Leonard, *J. Am. Chem. Soc.* **1982**, *104*, 5497; b) A. M. Halpern, M. A. Rossman, R. S. Hosmane, N. J. Leonard, *J. Phys. Chem.* **1984**, *88*, 4324; c) M. Shahbaz, S. Urano, P. R. LeBreton, M. A. Rossman, R. S. Hosmane, N. J. Leonard, *J. Am. Chem. Soc.* **1984**, *106*, 2805.
[17] D. D. Cubicciotti, W. M. Latimer, *J. Am. Chem. Soc.* **1948**, *70*, 3509.
[18] C. Grundmann, A. Kreutzberger, *J. Am. Chem. Soc.* **1955**, *77*, 6559.
[19] a) A. I. Finkel'shtein, N. V. Spiridova, *Russ. Chem. Rev.* **1964**, *33*, 400; b) A. I. Finkel'shtein, *Opt. i Spektr.* **1959**, *6*, 17.
[20] a) M. K. Marchewka, *Bull. Korean Chem. Soc.* **2004**, *25*, 466; b) M. K. Marchewka, *J. Chem. Res. Synop.* **2003**, 518; c) P. J. Larkin,

  

M. P. Makowski, N. B. Colthoup, *Spectrochim. Acta* **1999**, *55*, 1011; d) W. Jeremy-Jones, W. J. Orville-Thomas, *Trans. Faraday Soc.* **1959**, *55*, 193; e) E. N. Boitsov, A. I. Finkel'shtein, *Russ. Chem. Rev.* **1962**, *31*, 712.

[21] a) M. Takimoto, *Kogyo Kagaku Zasshi* **1961**, *64*, 1452; b) M. Takimoto, *Kogyo Kagaku Zasshi* **1964**, *85*, 168.

[22] B. V. Lotsch, W. Schnick, *Chem. Eur. J.* DOI: 10.1002/chem.200601291.

[23] V. V. Khorosheva, A. I. Finkel'shtein, *Zh. Fiz. Khim.* **1962**, *36*, 1055.

[24] B. Jürgens, Ph. D. thesis, University of Munich (Germany), Shaker, Aachen, **2004**.

[25] C. Gervais, F. Babonneau, J. Maquet, C. Bonhomme, D. Massiot, E. Framery, M. Vaultier, *Magn. Reson. Chem.* **1998**, *36*, 407.

[26] a) A. Sattler, Diploma thesis, University of Munich (Germany), **2005**; b) A. Sattler, L. Seyfarth, J. Senker, W. Schnick, *Z. Anorg. Allg. Chem.* **2005**, *631*, 2545.

[27] J. Sehnert, K. Bärwinkel, J. Senker, *J. Phys. Chem. B*, **2007**, submitted.

[28] a) T. E. Weirich, X. Zou, R. Ramlau, A. Simon, G. L. Cascarano, C. Giacovazzo, S. Hovmöller, *Acta Crystallogr. Sect. A* **2000**, *56*, 29; b) T. E. Weirich, R. Ramlau, A. Simon, S. Hovmöller, X. Zou, *Nature* **1996**, *382*, 144; c) U. Kolb, G. N. Matveeva, *Z. Kristallogr.* **2003**, *218*, 259; d) T. E. Weirich, J. Portillo, G. Cox, H. Hibst, S. Nicolopoulos, *Ultramicroscopy* **2006**, *106*, 164; e) D. L. Dorset, C. J. Gilmore, *Acta Crystallogr. Sect. A* **2000**, *56*, 62; f) D. L. Dorset, *Z. Kristallogr.* **2003**, *218*, 458; g) R. Vincent, P. A. Midgeley, *Ultramicroscopy* **1994**, *53*, 271.

[29] a) A. Altomare, M. C. Burla, M. Camalli, G. L. Cascarano, C. Giacovazzo, A. Guagliardi, A. G. G. Moliterni, G. Polidori, R. Spagna, *J. Appl. Crystallogr.* **1999**, *32*, 115; b) A. Altomare, G. L. Cascarano, C. Giacovazzo, A. Guagliardi, *J. Appl. Crystallogr.* **1993**, *26*, 343.

[30] M. S. Weiss, *J. Appl. Crystallogr.* **2001**, *34*, 130.

[31] The structure solution was verified by using precession intensity data. Owing to their robustness with respect to sample misalignment and less pronounced dynamical effects, the data quality obtained under otherwise identical experimental conditions can be improved. Accordingly, $R_{rim}$ is 20% and the straightforward structure solution has a figure of merit of 19.5%. The structure refinement (184 independent reflections, no. of reflections/parameter $\approx 6$, $d_{min.}$ 0.78 Å) was less successful due to the large sample thickness, which gives rise to stronger dynamical effects (cf. Figure 11, middle).

[32] a) C. Janiak, *J. Chem. Soc. Dalton Trans.* **2000**, 3885; b) C. A. Hunter, J. M. Sanders, *J. Am. Chem. Soc.* **1990**, *112*, 5525.

[33] a) J. M. Cowley, *Acta Crystallogr.* **1961**, *14*, 920; b) J. M. Cowley, A. Goswami, *Acta Crystallogr.* **1961**, *14*, 1071.

[34] J. J. P. Stewart, *J. Comput. Chem.* **1989**, *10*, 221.

[35] Gaussian 03, Revision C.02, M. J. Frisch, G. W. Trucks, H. B. Schlegel, G. E. Scuseria, M. A. Robb, J. R. Cheeseman, J. A. Montgomery, Jr., T. Vreven, K. N. Kudin, J. C. Burant, J. M. Millam, S. S. Iyengar, J. Tomasi, V. Barone, B. Mennucci, M. Cossi, G. Scalmani, N. Rega, G. A. Petersson, H. Nakatsuji, M. Hada, M. Ehara, K. Toyota, R. Fukuda, J. Hasegawa, M. Ishida, T. Nakajima, Y. Honda, O. Kitao, H. Nakai, M. Klene, X. Li, J. E. Knox, H. P. Hratchian, J. B. Cross, V. Bakken, C. Adamo, J. Jaramillo, R. Gomperts, R. E. Stratmann, O. Yazyev, A. J. Austin, R. Cammi, C. Pomelli, J. W. Ochterski, P. Y. Ayala, K. Morokuma, G. A. Voth, P. Salvador, J. J. Dannenberg, V. G. Zakrzewski, S. Dapprich, A. D. Daniels, M. C. Strain, O. Farkas, D. K. Malick, A. D. Rabuck, K. Raghavachari, J. B. Foresman, J. V. Ortiz, Q. Cui, A. G. Baboul, S. Clifford, J. Cioslowski, B. B. Stefanov, G. Liu, A. Liashenko, P. Piskorz, I. Komaromi, R. L. Martin, D. J. Fox, T. Keith, M. A. Al-Laham, C. Y. Peng, A. Nanayakkara, M. Challacombe, P. M. W. Gill, B. Johnson, W. Chen, M. W. Wong, C. Gonzalez, and J. A. Pople, Gaussian, Inc., Wallingford CT, **2004**.

[36] M. D. Segall, P. J. D. Lindan, M. J. Probert, C. J. Pickard, P. J. Hasnip, S. J. Clark, M. C. Payne, *J. Phys. Condens. Matter* **2002**, *14*, 2717.

[37] S. L. Mayo, B. D. Olafson, W. A. Goddard III, *J. Phys. Chem.***1990**, *94*, 8897.

[38] a) B. Delley, *J. Chem. Phys.* **1990**, *92*, 508; b) B. Delley, *J. Chem. Phys.* **2000**, *113*, 7756.

[39] J. E. Lowther, *Phys. Rev. B*, **1999**, *59*, 11683.

[40] E. Horvath-Bordon, R. Riedel, P. F. McMillan, P. Kroll, G. Miehe, P. A. van Aken, A. Zerr, P. Hoppe, O. Shebanova , I. McLaren, S. Lauterbach, E. Kroke, R. Boehler, *Angew. Chem.* **2007**, *119*, 1498; *Angew. Chem. Int. Ed.* **2007**, *46*, 1476 .

[41] A. E. Bennett, C. Rienstra, M. Auger, K. V. Lakshmi, R. G. Griffin, *J. Chem. Phys.* **1995**, *103*, 6951.

[42] S. Zhang , X. Wu , M. Mehring, *Chem. Phys. Lett.* **1990**, *173*, 481.

[43] Y. Ishii, *J. Chem. Phys.* **2001**, *114*, 8473.

[44] a) X. D. Zou, Y. Sukharev, S. Hovmöller, *Ultramicroscopy* **1993**, *49*, 147; b) X. D. Zou, Y. Sukharev, S. Hovmöller, *Ultramicroscopy* **1993**, *52*, 436.

[45] S. Weber, *Java Structure Viewer*, v1.08, 1999.

[46] Z. H. Wan, Y. D. Liu, Z. Q. Fu, Y. Li, T. Z. Cheng, F. H. Li, H. F. Fan, *Z. Kristallogr.* **2003**, *218*, 308.

[47] P. A. Stadelmann, *Ultramicroscopy* **1987**, *21*, 129.

[48] G. M. Sheldrick, SHELX-97, Programs for the solution and the refinement of crystal structures, University of Göttingen, Göttingen (Germany), **1997**.

[49] P. A. Doyle, P. S. Turner, *Acta Crystallogr. A* **1968**, *24*, 390.

Received: December 7, 2006
Published online: April 5, 2007

  